Supporting Information

Mn(II) Complex Impregnated Porous Silica Nanoparticles as Zn(II)-Responsive "Smart" MRI Contrast Agent for Pancreas Imaging

*Riya Mallik, Muktashree Saha, Vandna Singh, Hari Mohan, S. Senthil Kumaran, and Chandan Mukherjee**

Contents	Page
^{1}H NMR, ^{13}C NMR spectra, ESI-MS (+ve) and FTIR plots for ligand H_2AlcDPA	S2-S3
FTIR plots for ligand Complex **1**	S4
^{1}H NMR, ^{13}C NMR spectra, ESI-MS (+ve) and FTIR plots for ligand HPy_2Pic	S5-S6
Experimental and simulated curves representing pH-potentiometric titration of ligand H_2AlcDPA and Hpy_2Pic solution, in 0.15 M NaCl and 25 °C	S7
UV-Vis spectra of Complex **1** at pH ~ 7.4 and pH ~ 10.1, and 25 °C	S8
Morphological characterization of Complex **1**@SiO_2-NH_2NPs and Complex **1**@SiO_2-Py_2PicNPs	S8-S9
FTIR spectra for Complex **1**@SiO_2-Py_2PicNPs, lyophilized from water and D_2O medium, in the presence of BSA and Zn(II) ions	S9-S10
Relaxometric studies of different synthesized nanomaterials	S10-S12
TGA and zeta potential studies for BSA and Zinc ion interaction with Complex **1**@SiO_2-Py_2PicNPs	S13
Fluorescence quenching studies of BSA by Complex **1**@SiO_2-Py_2PicNPs and Zinc ions	S14
Biodistribution of Mn in different organ tissues, post *in-vivo* administration of synthesized nanomaterials	S15
Number of Complexes per Nanoparticle	S15
Fluorescence quenching study	S16
Selected bond distances (Å) and bond angles (°) for Complex **1**	S16
Ligand protonation constants and corresponding stability constants for some Mn(II) complexes	S17
Complex **1**@SiO_2-Py_2PicNPs•BSA•Zn(II) interaction studies	S17
Crystallographic data and structure refinement parameters for ligand H_2PyDPA and Complex **1**	S18

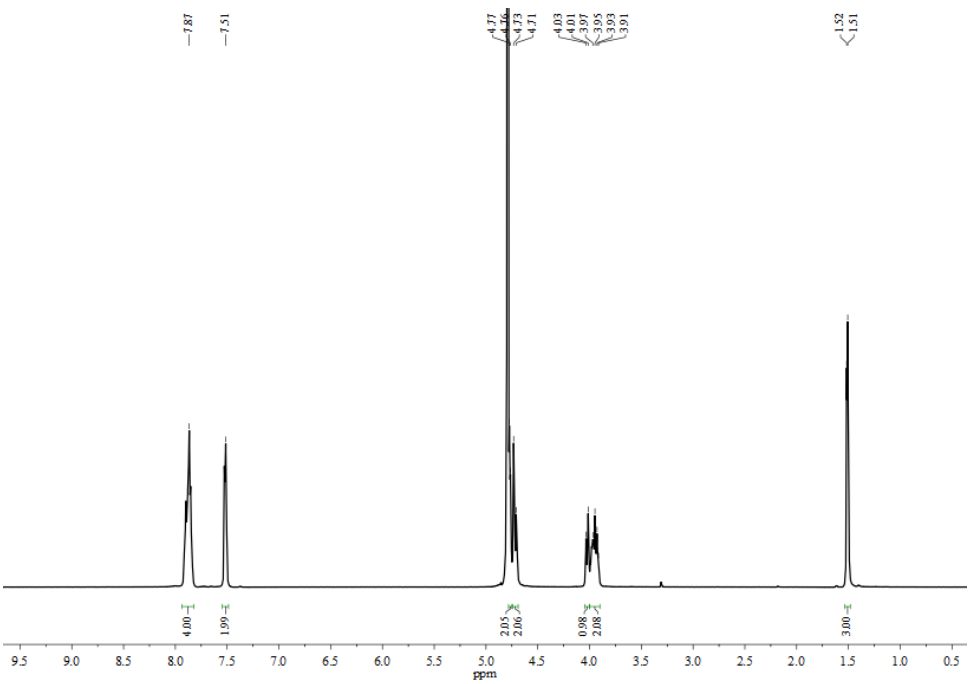

Figure S1. ^{1}H-NMR spectrum of ligand H_2AlcDPA•HCl in D_2O solvent.

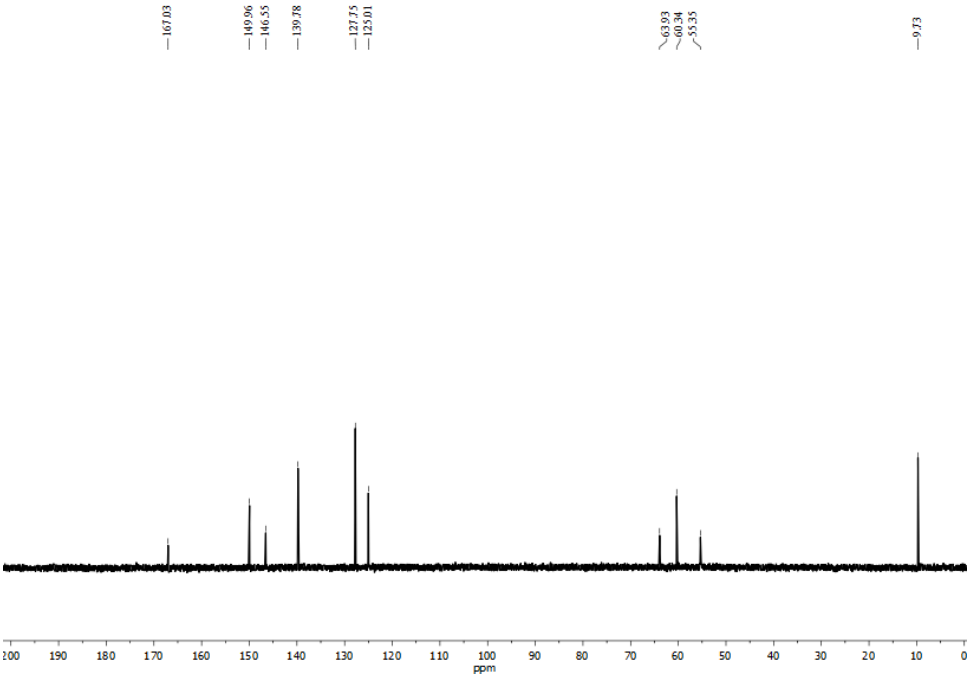

Figure S2. ^{13}C-NMR spectrum of ligand H_2AlcDPA•HCl in D_2O solvent.

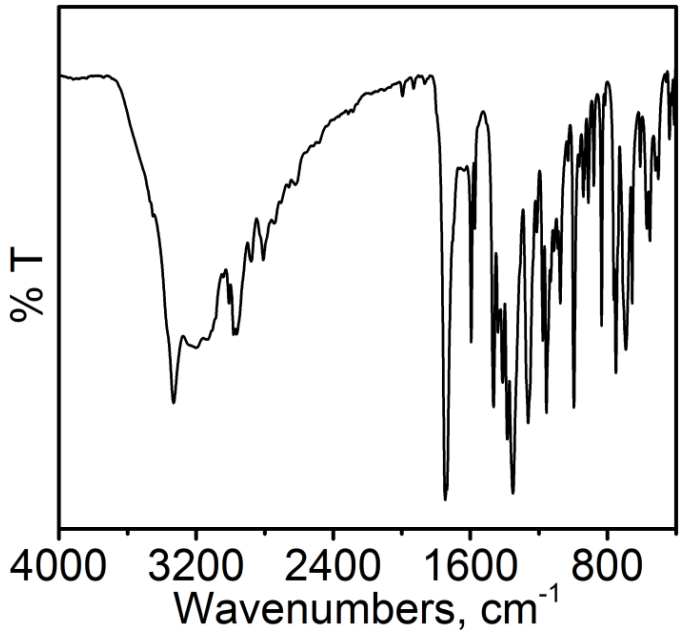

Figure S3. FTIR spectrum of ligand H_2AlcDPA•HCl.

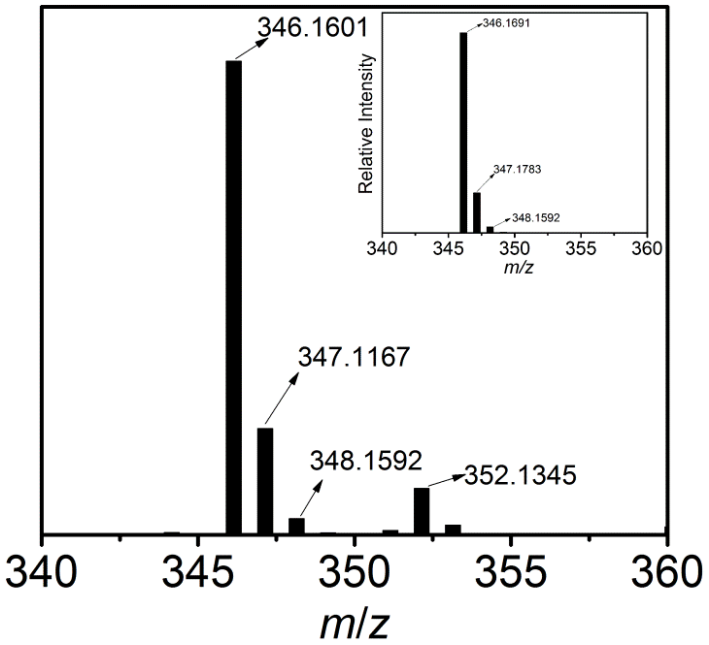

Figure S4. ESI-MS (+ve) mass spectrum of aqueous solution of ligand H_2AlcDPA•HCl. Simulated spectrum has been given as inset.

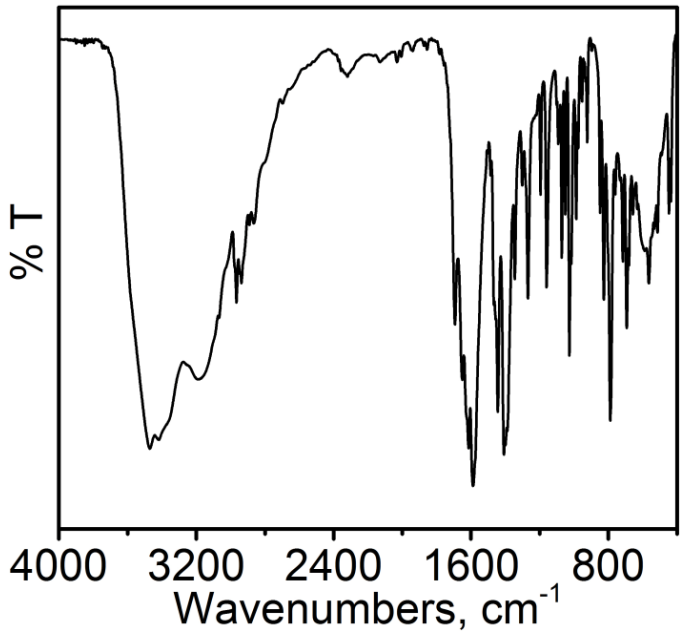

Figure S5. FTIR spectrum of Complex **1**.

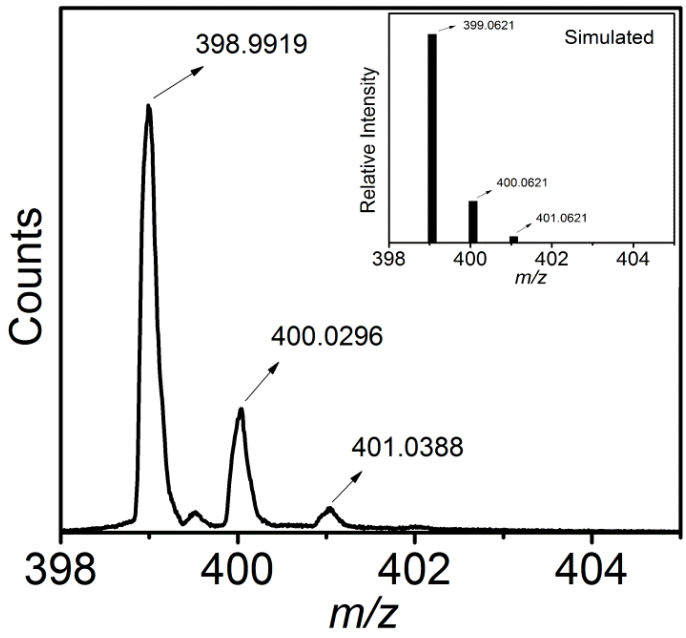

Figure S6. ESI-MS (+ve) mass spectrum of Complex **1**. Simulated spectrum has been been given as inset.

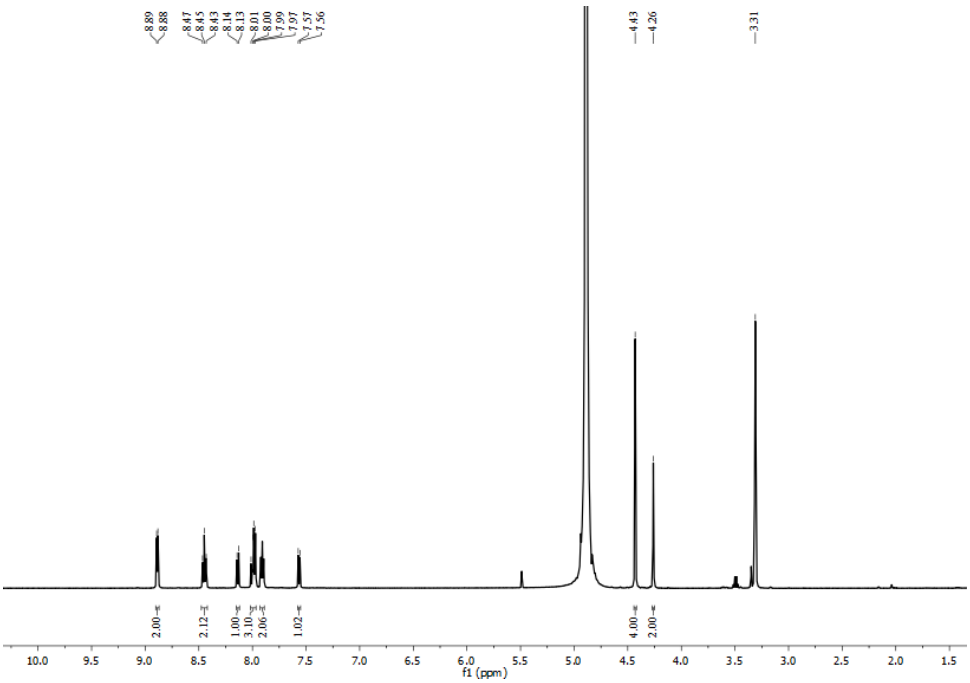

Figure S7. ^{1}H-NMR spectrum of ligand $HPy_2Pic{\bullet}HPF_6$ in CD_3OD solvent.

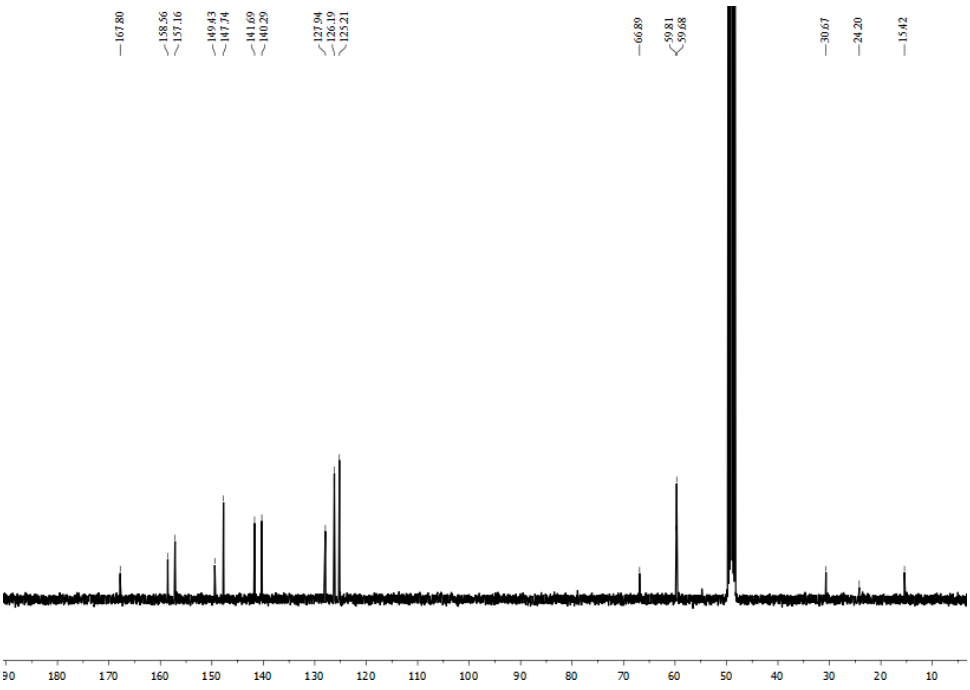

Figure S8. ^{13}C-NMR spectrum of ligand $HPy_2Pic{\bullet}HPF_6$ in CD_3OD solvent.

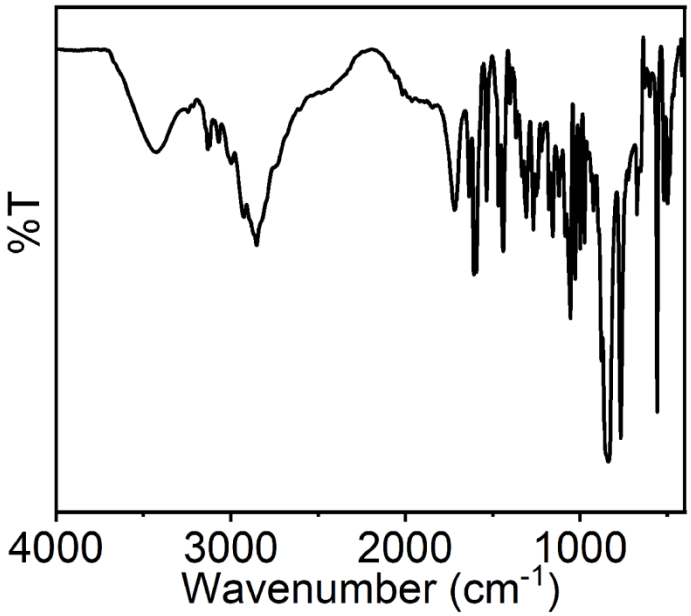

Figure S9. FTIR spectrum of ligand $HPy_2Pic{\bullet}HPF_6$.

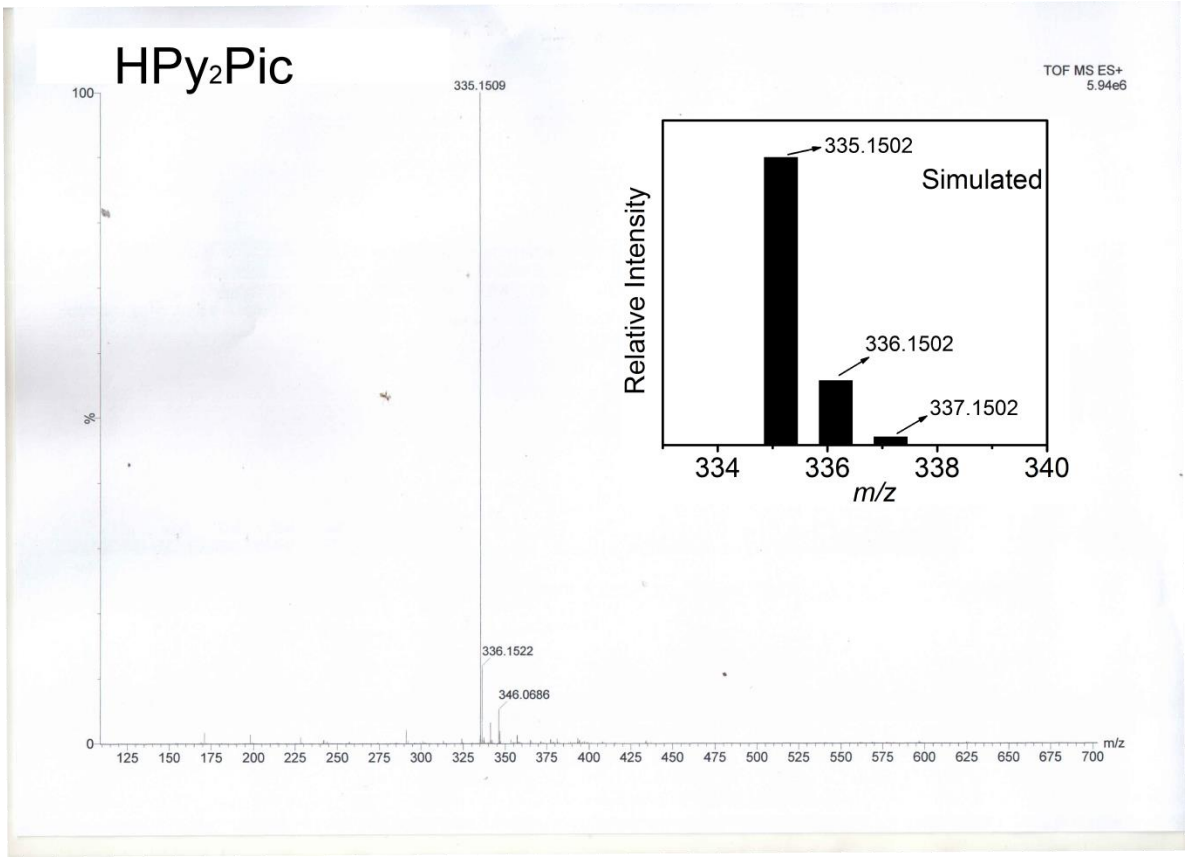

Figure S10. ESI-MS (+ve) mass spectrum of aqueous solution of ligand $HPy_2Pic{\bullet}HPF_6$. Simulated spectrum has been given as inset.

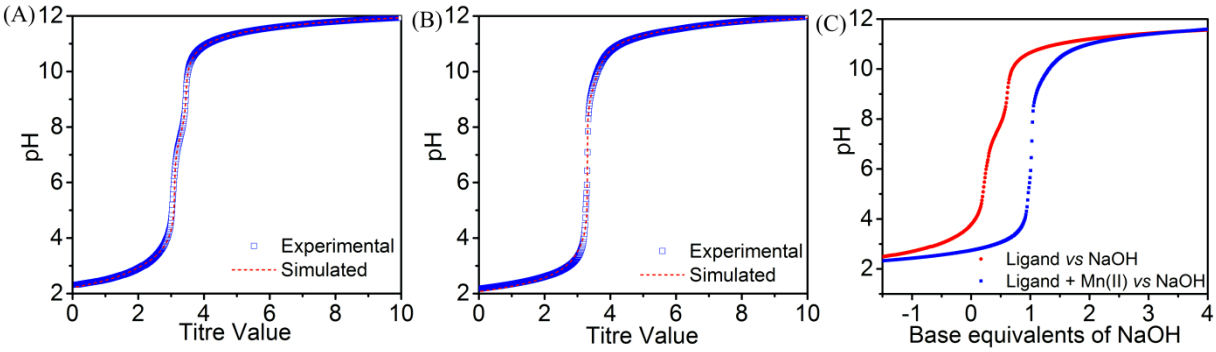

Figure S11: Experimental and simulated curves representing pH-potentiometric titration of (A) ligand H_2AlcDPA solution, and (B) ligand H_2AlcDPA:Mn(II) (1:1) solution against standard NaOH solution in 0.15 M NaCl and 25 °C. (C) Potentiometric titration curves of the ligand H_2AlcDPA solution with 1 equivalent of $MnCl_2 \bullet 4H_2O$ salt in H_2O in 0.15 M NaCl, and 25 °C.

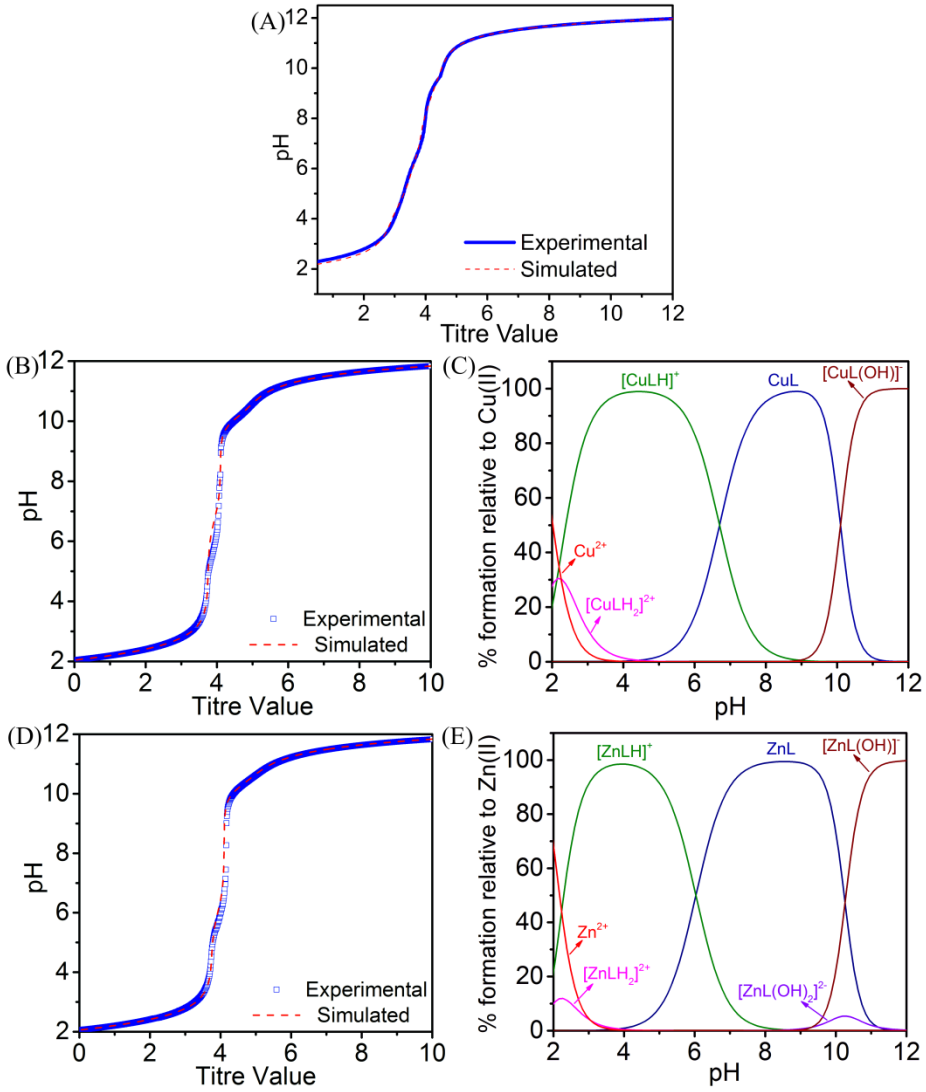

Figure S12: Experimental and simulated curves representing pH-potentiometric titration of (A) ligand HPy_2Pic solution, (B) ligand HPy_2Pic:Cu(II) (1:1) solution and (D) ligand HPy_2Pic:Zn(II) (1:1) solution against standard NaOH solution in 0.15 M NaCl and 25 °C. (C) and

(E) represented corresponding species distriction plots for HPy_2Pic:Cu(II) and HPy_2Pic:Zn(II) systems, respectively.

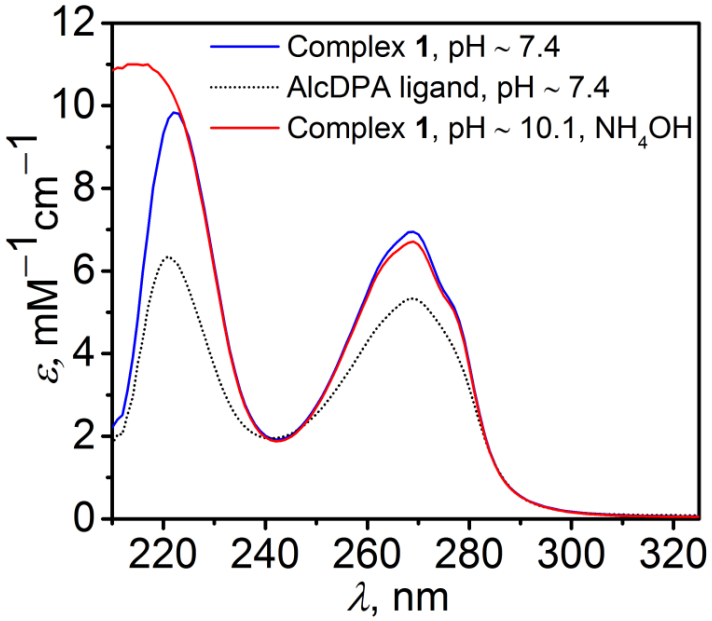

Figure S13: UV-Vis spectroscopy of Complex **1** at pH ~ 7.4 and pH ~ 10.1 (attained by addition of NH_4OH), and 25 °C.

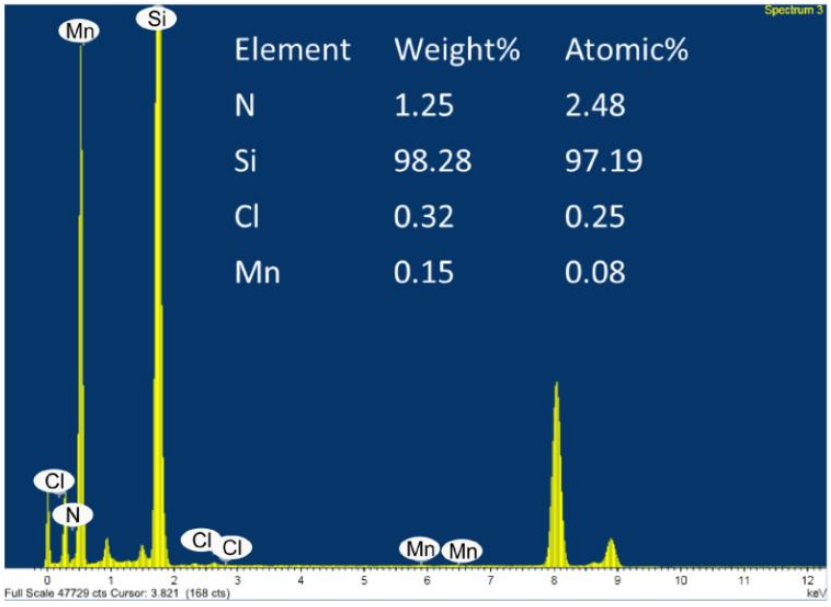

Figure S14. Morphological characterization of Complex **1**@SiO_2-NH_2NPs: Energy dispersive X-ray (EDS) analysis of Complex **1**@SiO_2-NH_2NPs showing existence of Mn, Si, N and Cl elements in the isolated nanoparticles.

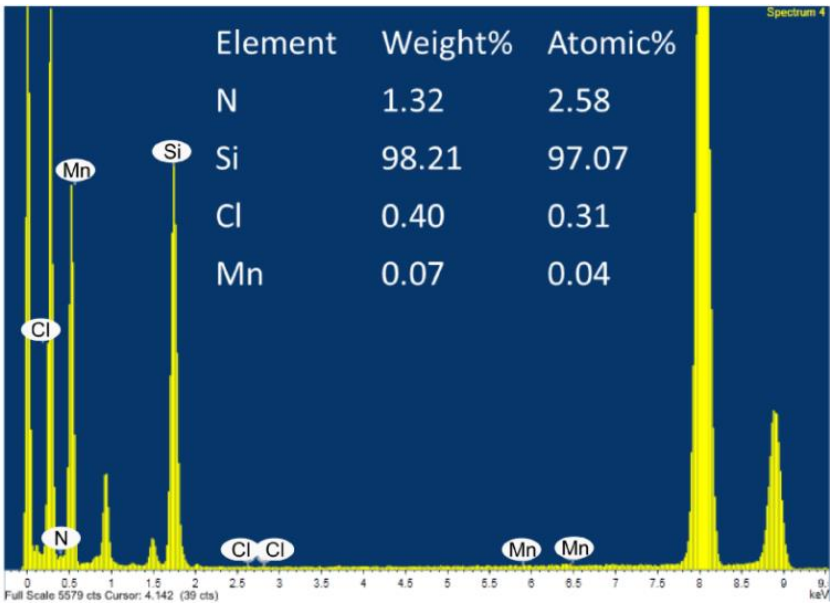

Figure S15. Morphological characterization of Complex **1**@SiO_2-Py_2PicNPs: Energy dispersive X-ray (EDS) analysis of Complex **1**@SiO_2-Py_2PicNPs showing existence of Mn, Si, N and Cl elements in the isolated nanoparticles.

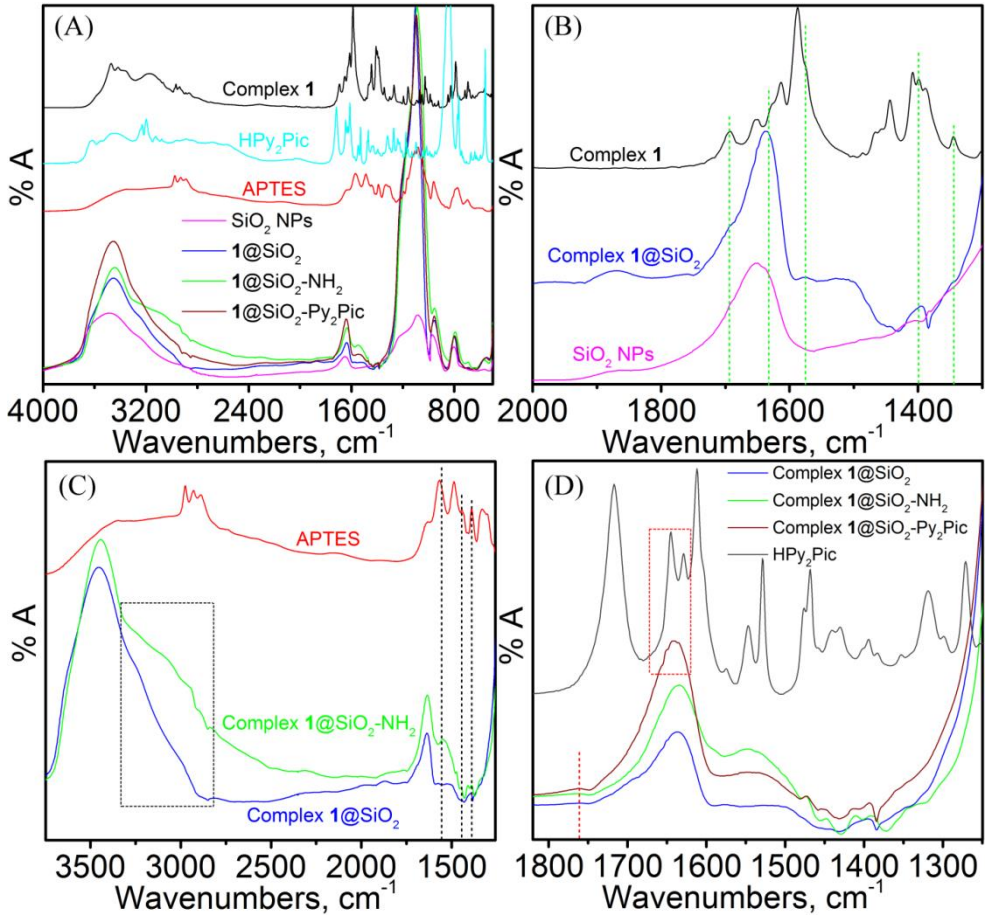

Figure S16. (A) FTIR spectra of Complex **1**@SiO_2NP, Complex **1**@SiO_2-NH_2NP, and Complex **1**@SiO_2-Py_2PicNP compared to the spectra for pristine SiO_2 NPs, Complex **1**, HPy_2Pic and APTES. (B)-(D) Zoomed in regions.

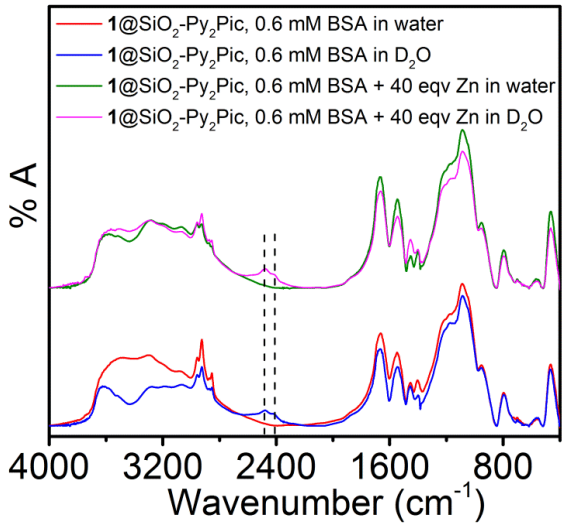

Figure S17. FTIR spectra of lyophilized Complex **1**@SiO_2-Py_2PicNP, recovered after suspending in 0.6 mM BSA solution in water (red line), in 0.6 mM BSA solution in D_2O (blue line), in 0.6 mM BSA and 40 eqv. Zn(II) solution in water (green line), and in 0.6 mM BSA and 40 eqv. Zn(II) solution in D_2O (pink line).

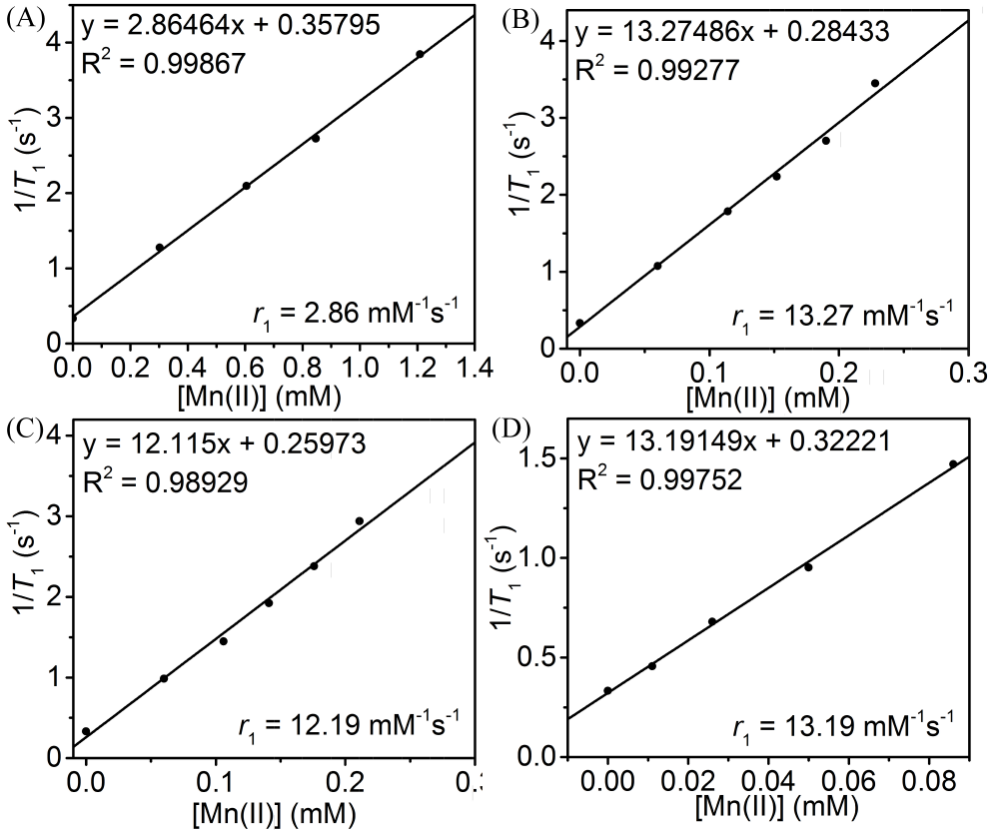

Figure S18: $1/T_1$ *vs* [Mn(II)] plot for (A) Complex **1**, (B) Complex **1**@SiO_2, (C) Complex **1**@SiO_2-NH_2NP, and (D) Complex **1**@SiO_2-Py_2PicNP. Experiments were done at 1.41 T, 37 °C, and pH ~ 7.4.

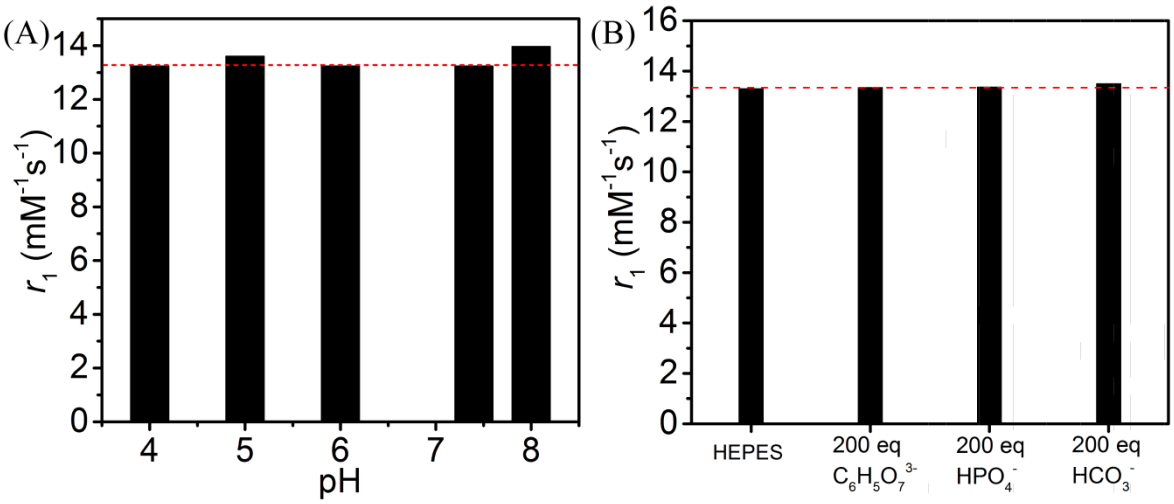

Figure S19: r_1 values for Complex **1**@SiO_2-Py_2PicNP suspension, (A) in the pH range 4.0-8.0, and (B) in the presence of 200 equivalents excess of different physiologically relevant anions, at pH 7.4; [Mn(II)] = 0.1 mM.

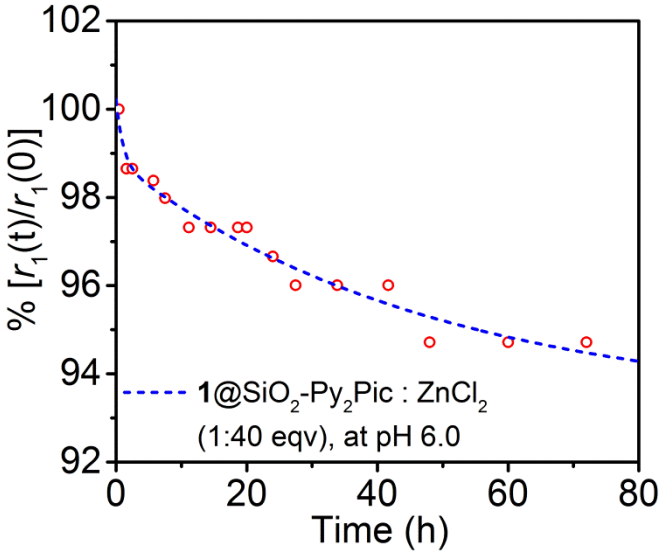

Figure S20. Time dependent longitudinal relaxivity study of Complex **1**@SiO_2-Py_2PicNP suspension challenged with 40 equivalents excess of Zn(II) ion. Experiment was performed with sample containing [Mn(II)] = 0.1 mM, dispersed in MES buffer, pH ~ 6.0, 1.41 T, at 37 °C.

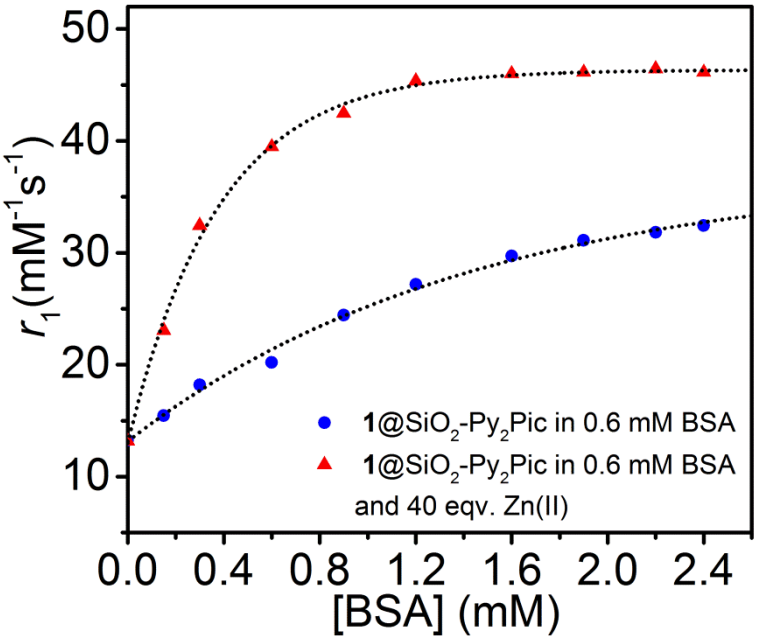

Figure S21. Relaxometric titrations of Complex **1**@SiO_2-Py_2PicNP (0.06 mM Mn(II) concentration) as a function of increasing concentration of BSA, in the absence and presence of 40 equiv. excess of Zn(II) ions. Measurements were done at pH ~ 7.4, 1.41 T, and 37 °C.

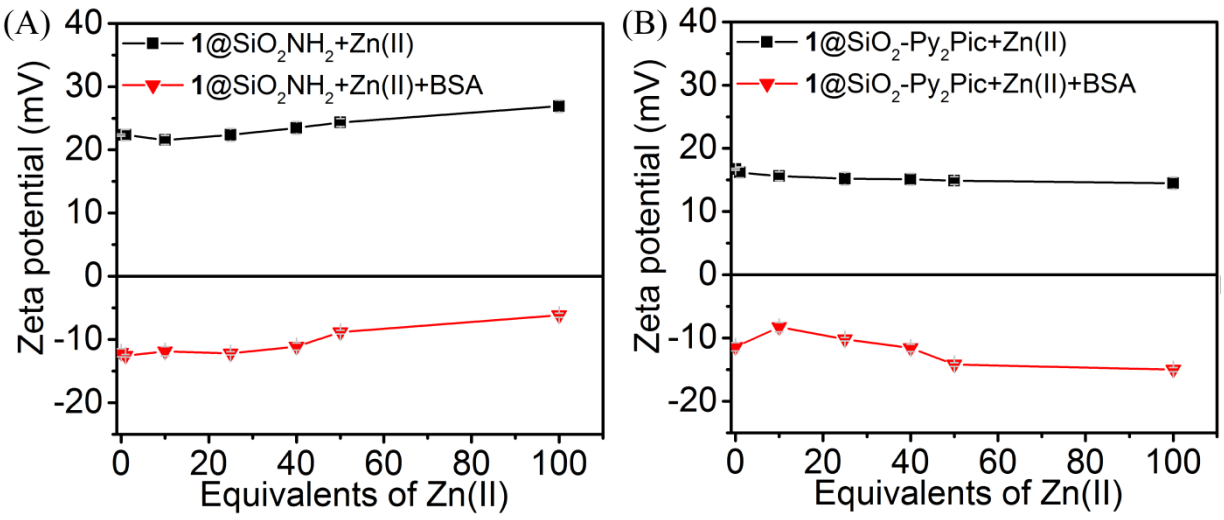

Figure S22. Zeta potential changes of (A) Complex **1**@SiO_2-NH_2NP and (B) Complex **1**@SiO_2-Py_2PicNP with increasing equivalents of Zn(II), in the absence and presence of 0.6 mM BSA, at pH ~ 7.4.

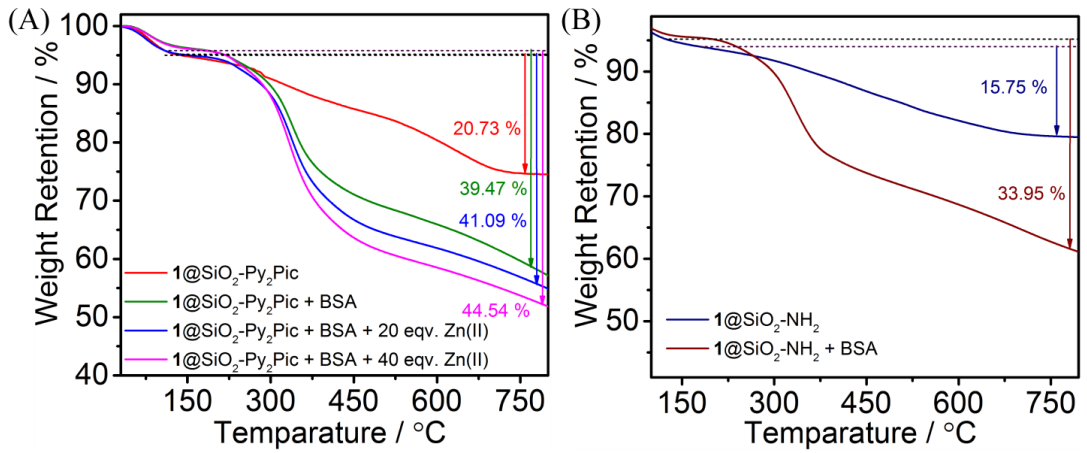

Figure S23: TGA analysis spectra for (A) Complex **1**@SiO_2-Py_2PicNP lyophilized solid obtained after isolating Complex **1**@SiO_2-Py_2PicNP from (i) water (red line), (ii) 0.6 mM BSA solution (green line), (iii) 0.6 mM BSA and 20 equiv. Zn(II) solution (blue line), and (iv) 0.6 mM BSA and 40 equiv. Zn(II) solution (pink line); (B) Complex **1**@SiO_2-NH_2NP lyophilized solid obtained after isolating Complex **1**@SiO_2-NH_2NP from (i) water (navy line) and (ii) 0.6 mM BSA (brown line).

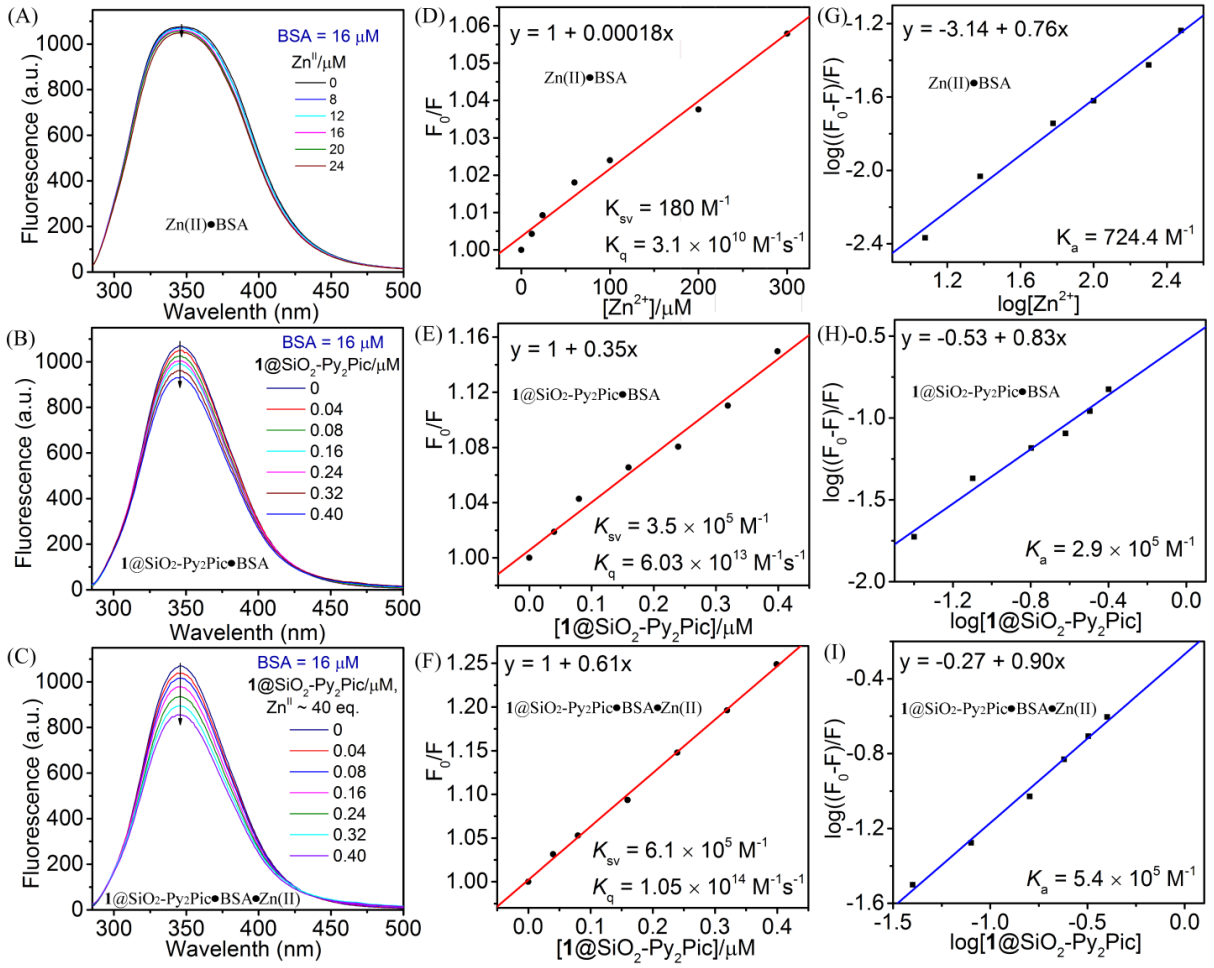

Figure S24. Estimation of Zn(II)•BSA, **1**@SiO_2-Py_2Pic•BSA and **1**@SiO_2-Py_2Pic:BSA•Zn(II) interactions by fluorescence spectroscopy. Fluorescence spectra of 16 μM BSA in the presence of increasing concentration of (A) Zn(II) ions, (B) **1**@SiO_2-Py_2PicNPs, and (C) Zn(II) ions and **1**@SiO_2-Py_2PicNPs together. Respective Stern-Volmer constant plots (D)-(F); and log (F_0-F)/F plots (G)-(I) to find out corresponding quenching constants (K_q) and affinity constants (K_a). Binding sites (n) was found to be equal to 1 in each case.

Figure S25. T_1-weighted axial images of mice showing contrast changes in urinary bladder pre and 1 hour post administration of Complex **1**@SiO_2-NH_2 or Complex **1**@SiO_2-Py_2Pic, without or with D-glucose (injected 45 min after contrast administration), at 7 T animal MR scanner.

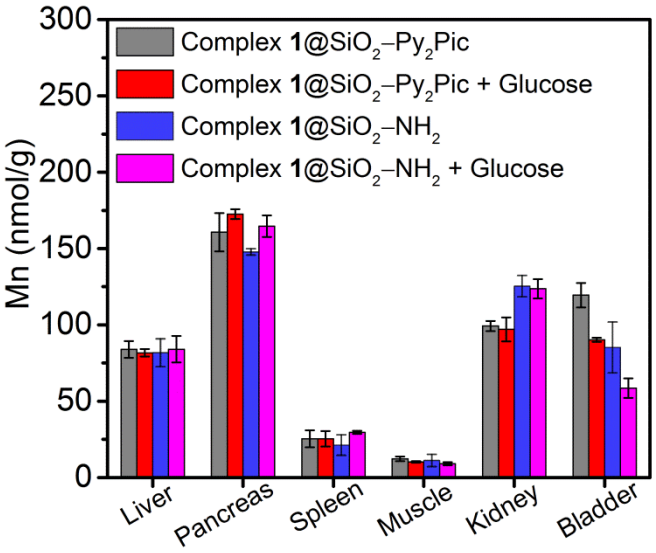

Figure S26. Manganese content in mice organ tissues, obtained by ICP-MS studies, 1 hour after intraperitoneal administration of respective contrast agents (10 μmol/kg *w.r.t.* [Mn(II)]) along without or with glucose (2.2 mmol/kg).

Number of Complexes per Nanoparticle.

The average number of complexes confined within each nanoparticle (Complex **1**@SiO_2NP) was determined using the formula:[1]

$$N_1 = \frac{cVN_A}{\eta/m_{NP}} = \frac{cVN_A(\frac{1}{6}\pi\rho_{NP}d^3)}{\eta} \qquad \textbf{(Equation S1)}$$

Where c = concentration in mother suspension,

V = volume of mother suspension,

N_A = Avogadro's number,

η = yield from synthesis,

m_{NP} = mass of nanoparticle,

ρ_{NP} = density of nanoparticle (considered same as that of pure silica, 1.95 g cm^{-3}),

d = diameter of nanoparticle.

500 μL of mother suspension was lyophilized for 24 h and 12 mg of dry silica were obtained. For Mn(II) concentration to be 0.29 mM and each nanoparticle sized 13.22 nm, n_{cplx} = 34.

Fluorescence quenching study.

Stern-Volmer equation:

$$F_0/F = 1 + K_{sv}[Q] = 1 + k_q \tau_0[Q] \quad \textbf{(Equation S2)}$$

F_0 and F are the maximum fluorescence intensities in the absence and presence of quencher, respectively. k_q is the bimolecular quenching constant, which is a measurement of the efficiency of quenching. τ_0 is the average lifetime of the Trp 214 unit and it is equal to 5.8×10^{-9} s.[2] [Q] is the quencher concentration.

$$\log[(F_0 - F)/F] = \log K_a + n\log[Q] \quad \textbf{(Equation S3)}$$

n is the number of binding sites and K_a represents the binding constant.

Table S1: Selected bond distances (Å) and bond angles (°) for complex **1**.

Mn1–O2	2.256(2)
Mn1–O3	2.280(2)
Mn1–O4	2.261(2)
Mn1–N1	2.276(2)
Mn1–N2	2.539(2)
Mn1–N3	2.251(2)
Mn1–Cl1	2.485(1)
O2–Mn1–O4	77.63(6)
O2–Mn1–N1	70.80(6)
N3–Mn1–O4	72.02(6)
N1–Mn1–N2	69.16(6)
N3–Mn1–N2	68.46(6)
O3–Mn1–Cl1	177.90(5)

Table S2: Ligand protonation constants and corresponding stability constants for Mn(II), Zn(II) and Cu(II) complexes.

		PyC3A[a]	PC2A-DPA[b]	AlcDPA[c]	Py_2Pic[c]
H^+	$\log K_1^H$	10.16	10.65	7.69(3)	9.52(7)
	$\log K_2^H$	6.39	6.55	3.75(2)	8.31(8)
	$\log K_3^H$	3.13	5.84	—	6.34(8)
	$\log K_4^H$	—	4.39	—	4.95(8)
	$\sum \log K_i^H$	19.68	16.49	11.45	29.12
Mn^{2+}	$\log K_{MnL}$	14.14	15.87	15.06(8)	—
	$\log K_{MnHL}$	2.43	4.14	3.53(10)	—
	pMn	8.17	8.79	9.56	—
Cu^{2+}	$\log K_{CuL}$	—	19.05	—	19.31(1)
	$\log K_{CuHL}$	—	3.63	—	6.70(1)
	$\log K_{CuH2L}$	—	—	—	2.14(3)
	pCu	—	—	—	10.59
Zn^{2+}	$\log K_{ZnL}$	—	—	—	19.76(1)
	$\log K_{ZnHL}$	—	—	—	6.03(8)
	$\log K_{ZnH2L}$	—	—	—	1.66(7)
	pZn	—	—	—	10.82

[a][3] (I= 0.15 M NaCl, 25 °C). [b][4] (I= 0.15 M NaCl, 25 °C). [c] This work (I= 0.15 M NaCl, 25 °C).

Table S3. Evaluation of interaction between Complex **1**@SiO_2-Py_2Pic and BSA, in the absence and presence of 40 equiv. excess Zn(II) ions by relaxometry, zeta potential, TGA, and fluorescence quenching studies.

Suspension medium	[(a)]r_1 ($mM^{-1}s^{-1}$)	ζ (mV)	TGA weight loss (%)	[(b)]r_1^{sat} ($mM^{-1}s^{-1}$)	[(c)]K_{sv} ($10^5\ M^{-1}$)	[(c)]K_q ($10^{13}\ M^{-1}s^{-1}$)	[(c)]K_a ($10^5\ M^{-1}$)
Water	13.19	16.6	20.73	—	—	—	—
BSA, 0.6 mM	20.18	-11.5	39.47	37.08	3.5	6.0	2.9
BSA, 0.6 mM and 40 equiv. Zn^{II} ions	39.01	-11.6	44.54	46.55	6.1	10.5	5.4

Relaxometric studies were done at pH 7.4, 1.41 T, and 37 °C. [(a)] Each relaxivity value was obtained from $1/T_1$ versus [Mn(II)] ([Mn(II)] = 0.02, 0.04, 0.08, 0.10 mM) plots with samples suspended in different medium, as mentioned. [Zn(II)] maintained at 40 equivalent excess amount, *w.r.t.* Mn(II) concentration. [(b)]Saturated relaxivity values obtained after fitting the titration curves of complex **1**@SiO_2-Py_2PicNP (0.06 mM Mn(II) concentration) with increasing concentration of BSA, in absence and presence of 40 equiv. excess of Zn(II) ions. [(c)]Binding sites (n) was found to be equal to 1 in each case.

Table S4: Crystallographic and Structural refinement parameters for complex **1**.

Empirical formula	$C_{34}H_{42}Cl_2Mn_2N_6Na_2O_{14}$
CCDC Number	2260190
Formula weight	985.49
Crystal habit, colour	Neddle-shaped/ colourless
Crystal size, mm^3	0.35×0.32×0.30
Temperature, *T*	293(2)
Wavelength, λ(Å)	0.71073
Crystal system	monoclinic
Space group	'P 21'
Unit cell dimension	*a* = 9.1405(3) Å, *b* = 13.8564(5) Å, *c* = 16.7601(6) Å, α = 90.00°, β= 105.4930°, γ = 90.00°
Volume, *V* ($Å^3$)	2045.61(12)
Z	2
Calculated density, $mg \bullet mm^{-3}$	1.600
Absorption coefficient, μ (mm^{-1})	0.843
F(000)	1012
θ range for data collection	2.93° to 27.28°
Limiting indices	-10≤*h* ≤10, -16≤*k*≤16, -19≤*l*≤19
Reflection collected / unique	48385/6849 [$R_{(int)}$ = 0.0257]
Completeness to θ	99.0% (θ = 25°)
Max. and min. transmission	0.7455/0.6402
Refinement method	'SHELXL-2018 (Sheldrick, 2018)'
Data / restrains / parameters	7098/1/578
Goodness-of-fit on F^2	1.062
Final *R* indices [*I*>2sigma(*I*)]	R_1 = 0.0211, wR_2 = 0.0552
R indices (all data)	R_1 = 0.0225, wR_2 = 0.0565
Largest diff. peak and hole	0.202/-0.227

REFERENCES

[1] S. V. Eliseeva, B. Song, C. D. B. Vandevyver, A. -S. Chauvin, J. B. Wacker and J. -C. G. Bünzli, *New J. Chem.* **2010**, *34*, 2915-2921.

[2] C. Moya, R. Escudero, D. C. Malaspina, M. de la Mata, J. Hernández-Saz, J. Faraudo, A. Roig, *ACS Appl. Bio Mater*. **2019**, *2*, 3084-3094.

[3] E. M. Gale, I. P. Atanasova, F. Blasi, I. Ay, P. Caravan, *J. Am. Chem. Soc.* **2015**, *137*, 15548−15557.

[4] R. Botár, E. Molnár, Z. Garda, E. Madarasi, G. Trencsényi, J. Kiss, F. K. Kálmán, G. Tircsó, *Inorg. Chem. Front*. **2022**, *9*, 577-583.